Machine-learning Based Reliability Analysis of Structural Concrete Cracking Considering Realistic Non-Uniform Corrosion Development

Xun Xi[1], Ziqing Yin[2], Shangtong Yang[3*] and Chun-Qing Li[4]

[1] Associate Professor, School of Civil and Resource Engineering, University of Science and Technology Beijing, Beijing 100083, China
[2] PhD Student, Department of Civil and Environmental Engineering, University of Strathclyde, Glasgow, G1 1XJ, United Kingdom
[3] Senior Lecturer, Department of Civil and Environmental Engineering, University of Strathclyde, Glasgow, G1 1XJ, United Kingdom
[4] Professor, School of Engineering, Royal Melbourne Institute of Technology University, Melbourne, VIC 3001, Australia.

ABSTRACT: Corrosion-induced concrete cracking significantly weakens the integrity, serviceability and durability of reinforced concrete (RC) structures. Existing reliability analysis of corrosion-induced concrete cracking often considers the corrosion of reinforcement as a uniform process, in favour of implementing the analytical formulation of corrosion rust progression. However, corrosion distribution in RC structures is seldom uniform around the steel reinforcement hence the corrosion-induced pressure. Thus, considering the non-uniform corrosion process in the reliability analysis becomes important. This paper develops a time-dependent reliability methodology, combining mesoscale heterogeneous fracture modelling and state-of-the-art machine learning algorithm, to assess the serviceability of the RC structures subjected to non-uniform development of corrosion. The effects of critical crack width, corrosion non-uniformity, and chloride content, temperature and relative humidity on the failure probability are investigated. The worked example demonstrates the importance of considering the non-uniformity of the corrosion product distribution, which provides reliable evaluation of the remaining safe life of RC structures comparing to the use of uniform corrosion model. The developed unified assessing methodology for corrosion of RC structures can serve as a useful tool for engineers, designers and asset managers for their decision-making with regard to repair and maintenance of corrosion-affected RC structures.

KEYWORDS: Non-uniform corrosion; Crack width; Reinforced concrete; Fracture mechanics; Reliability.

* Corresponding author. Tel: +44 141 548 3273. Email: shangtong.yang@strath.ac.uk.

1. INTRODUCTION

Reinforced concrete (RC) has been widely used in civil structures, e.g., ports, bridges, tunnels, offshore wind supporting foundations. However, due to chloride attacking from marine environment or de-icing, RC structures are susceptible to corrosion of the steel reinforcement [1, 2]. Corrosion rusts that consist of a matrix of iron oxy-hydroxides can expand at least 2-3 times compared with the original steel, leading to concrete cover cracking [3]. Corrosion-induced concrete cracking significantly threatens the serviceability of RC structures because it destroys the integrity of concrete cover, further accelerates the deterioration process and eventually causes catastrophic failure of the structures and infrastructure [4]. It has been reported that, 70–90% of practical cases for the deterioration of RC structures were dominated by corrosion of reinforcements [5]. Therefore, it is crucial to assess the failure risk considering corrosion-induced concrete cracking for the long-term serviceability of RC structures.

Typical approaches for modelling corrosion-induced concrete cracking includes empirical models regressed from experimental results [6, 7], analytical models based on fracture mechanics [8, 9], and numerical models based on the assumption of discrete or smeared cracks [10, 11]. However, due to mainly the limitations of experimental techniques and analytical solution to the governing partial differential equation, previous research has mainly considered the corrosion as a uniform process, i.e., corrosion products uniformly distribute and expand around the reinforcement [12]. However, in practice, reinforcement corrosion is rare to be uniform around the steel circumference due to the nature of chloride and oxygen diffusing into concrete from different sides of RC structures. Practical observations of corroded reinforcement have shown severe corrosion occurs in the part of reinforcement facing concrete cover [13, 14]. Yuan and Ji [15] measured the rust layer in RC specimens exposed to environmental chamber and proposed to use semi-elliptical shape and function to describe the non-uniform corrosion of reinforcement. Zhao et al. [16] developed the Gaussian model that is based on modified Gaussian function for describing the non-uniform rust layer. Qiao et

al. [17] proposed to model the non-uniform rust layer as a part of reinforcement uniformly corroded. Further, experimental results show that the non-uniform distribution of rust is not a constant shape but varies with RC structures and service environment [18-20].

Non-uniform corrosion brings difficulties to analytical methods for the determination corrosion-induced crack width due to the inability of deriving the closed-form solution after cracking initiation of concrete [9, 21]. Experimental and numerical approaches have been popular for investigating concrete cracking induced by non-uniform corrosion. Zhao et al. [22] carried out experiments to investigate the non-uniform corrosion induced cracks and obtained the relationship between crack width and steel loss ratio for the specimens. Qiao et al. [17] analysed the crack patterns caused by non-uniform corrosion by experiments and found the internal cracks in concrete was significantly affected by the corrosion distribution of rust. Chen et al. [23] carried out finite element modelling for corrosion-induced crack width propagation and found the crack width for non-uniform corrosion was much faster than that for uniform corrosion. Xi et al. [4] modelled corrosion-induced concrete cracking at meso-scale and found the crack width varied with different non-uniformity of corrosion products distribution. Chen et al. [18] investigated non-uniform rust development and concrete cracking by experiments and numerical simulations and found that the non-uniform development of rust was time-dependent and the crack width fluctuated with the corrosion development. The uncertainty of rust development poses a huge challenge for accurate prediction of corrosion-induced concrete cracking. Thus, current durability design of RC structures only considers the corrosion initiation time of reinforcement while the residual life from corrosion initiation to corrosion-induced limit crack width is not accounted for whole-life management of structures [24, 25].

Reliability analysis is an important method for the serviceability assessment and remaining lifetime prediction of RC structures affected by corrosion, due to the uncertainty of service environment and corrosion development. For reliability modelling of corrosion-induced concrete cracking, a physical failure criterion such as the crack width prediction model is necessary. There are three categories for crack width prediction: (1) analytical models based on fracture mechanics; (2) empirical models based

on experimentally established relationship between corrosion and crack width; and (3) numerical models. Li and Melchers [26] developed a time-dependent reliability model of corrosion-induced concrete cracking based on an analytical formulation in which corrosion development were simplified as uniform. Vu and Stewart [27] carried out time-dependent reliability analysis considering an empirical model of structural strength reduction caused by corrosion-induced concrete spalling. Zhang and Xiao [28-30] considered carbonation induced reinforcement corrosion in recycled aggregate concrete and carried out time-dependent reliability analysis on the carbonation behaviour based on gamma process. Biondini et al. [31] evaluated the lifetime structural performance of RC structures by time-dependent reliability analysis based on the reduction of steel cross-section for uniform corrosion. Val [32] proposed to use a pitting corrosion model for steel cross-section reduction to evaluate time-dependent reliability of RC structures and an empirical pitting corrosion model was employed. Gu et al. [2] developed a time-dependent reliability model by considering the non-uniformity of corroded steel bar and corresponding mechanical degradation of steel bar. Akiyama et al. [33] proposed a framework for estimating structural capacity and reliability based on corrosion-induced crack width from simulations. Zhang et al. [34] employed an empirical model to predict the remaining lifetime from corrosion initiation to corrosion-induced limit crack width for time-dependent reliability analysis.

However, there is currently no analytical model for predicting concrete crack width induced by non-uniform corrosion. Due to the uncertainty of corrosion, it is difficult to control corrosion rust non-uniformity and establish an accurate empirical model for the relationship between crack width and corrosion degree. Therefore, reliability analysis based on numerical method for non-uniform corrosion induced concrete cracking is a feasible approach. However, advanced yet computationally demanding numerical methods are not appropriate for direct incorporation with a reliability framework due to high computational cost and difficulties in deriving the explicit relationship between the crack width development and the underlying factors. For this reason, an efficient and implicit approach to evaluate the stochastic variables in the limit state equation is needed. Machine

learning algorithms based on numerical results can provide an effective solution for reliability modelling of non-uniform corrosion induced concrete cracking . To date, as far as the authors are aware, there is no reliability analysis considering the uncertainty of corrosion rust non-uniformity and concrete cracking, which adds inaccuracies in the assessment, maintenance and repair of RC structures affected by corrosion.

This paper develops a time-dependent reliability methodology for non-uniform corrosion induced concrete cracking. Advanced meso-scale numerical simulations for concrete fracture propagation induced by non-uniform corrosion of steel reinforcement are first conducted. The simulated crack width development is then validated with the available experimental results. A stochastic non-uniform corrosion model and a corrosion rate model from existing code of practice are combined with the advanced meso-scale numerical modelling for the prediction of the concrete crack growth. The developed database provides the underpinning input to the state-of-the-art machine learning algorithm (e.g., artificial neural network) and train a computationally efficient surrogate model suitable for Monte Carlo Simulation (MCS). The MCS is performed considering the randomness of the non-uniform coefficient, which is described by a probabilistic model developed from experimental data. The proposed methodology considers the uncertainty of corrosion non-uniformity and employs data-driven surrogate model which alleviates the computational burden of Monte Carlo Simulation.

2. METHODOLOGY

2.1 Stochastic non-uniform corrosion model

When RC structures are in service in marine environment or other corrosive environments, chloride, oxygen and moisture can usually penetrate the concrete cover and corrode the steel reinforcement, especially in the splash zone. Corrosion initiation will occur once the chloride content around the steel bar reaches the threshold value. Figure 1 illustrates two typical rust distributions around the steel bar. The corrosion products (thickness T_{cl} in Figure 1) will normally lead to 2-3 times expansion than

the corroded steel (thickness $T_{co\text{-}st}$ in Figure 1) [3]. The corrosion rust will first fill into a "porous zone" or "corrosion accommodating region" (normally 10-20 μm in thickness) between the concrete and steel bar (T_0 in Figure 1) [12]. Further, the growing rust will generate excessive expansion force and cause displacement of concrete cover, leading to concrete cover cracking usually in the longitudinal direction. The uniform corrosion model assumes corrosion products are uniformly distributed around the steel bar, which had been widely used for corrosion-induced concrete cracking studies [8, 10]. However, it is rare to have simultaneous corrosion initiation around the steel bar and the corrosion progression. Through more quantitative experimental investigations [15, 17, 19, 20], it has been found that more corrosion products are deposited at the part of reinforcement facing concrete cover surface due to shorter transportation routines of chloride and other ions. As such, non-uniform corrosion models have been proposed recently and used for determining the corrosion-induced concrete cracking [4, 20, 35, 36]. In this study, the non-uniform corrosion normally refers to the general corrosion and rather than the very localised pitting corrosion [37].

Xi and Yang [4] proposed a non-uniform corrosion model based on von Mises distribution, which is described as follows:

$$T_{cl}(\theta) = \alpha\pi R\eta \times \frac{e^{k\cos(\theta-\mu)}}{2\pi I_0(k)} \quad (1)$$

where α is the expansion ratio of rust to corroded steel; R is the radius of steel bar; η is the steel loss ratio or corrosion degree; k is the non-uniform coefficient (i.e., non-uniformity of corrosion products distribution); μ is the location where the maximum thickness of corrosion layer appears; I_0 is the modified Bessel function of order 0.

In the von Mises corrosion model, μ is very close to π in the polar coordination systems for both reinforcements located in the corner and middle of concrete [4]. It should be mentioned that, the right part after the multiplication in Equation (1) is the original form of von Mises distribution [38]. k is the non-uniform coefficient of corrosion with a positive value. A larger value of k represents a greater non-uniformity of the corrosion product distribution. Specially, k=0 represents the uniform corrosion.

Figure 2 shows the distributions of corrosion products for several cases of different *k*. It can be seen that, the corroded part of the steel bar is smaller if the value of *k* is larger. The rust is more concentrated facing the concrete cover surface. With the same corrosion degree (e.g., 0.5%), the maximum value of rust thickness for *k*=5 is about 0.4 mm which is more than twice of that for *k*=1. It can be predicted that the uniformity coefficient *k* will affect corrosion-induced concrete cracking time and crack width development.

Compared with other non-uniform models [15, 17, 19, 39, 40], von Mises corrosion model describes corrosion non-uniformity by the parameter *k*, which brings advantages to investigate the reliability of non-uniform induced concrete cracking by considering the non-uniformity as a random variable. Xi and Yang obtained the distribution of *k* for the steel bar in concrete samples through X-ray CT scanning [20]. The accelerated corrosion was finished by the wetting and drying cycles in a chloride environment. Figure 3 shows a three-parameter log-logistic probability density of non-uniform coefficient *k* which is developed based on the experimental data of 449 cross-sections of the steel bar. It can be seen that, the non-uniform coefficient varies from 2 to 11 and concentrates at 3 to 4.5. The fitted coefficients of the probability density function is given as follows:

$$f(x) = \frac{1}{B}\frac{1}{(x-C)}\frac{exp\left[\frac{ln(x-C)-A}{B}\right]}{\left\{1+exp\left[\frac{ln(x-C)-A}{B}\right]\right\}^2} \tag{2}$$

where $A = 0.6517$, $B = 0.3491$, $C = 1.7030$.

It should be mentioned that, it is very challenging to determine the value of *k* because the critical corrosion degree to concrete cracking is only a few thousandths and hard to be measured [18, 26, 41]. Existing experimental data on the randomness of *k* are very limited. To further verify the rationality of the random *k*, we collected the experimental data in the literature on rust distributions for the *k* values [15, 17-19]. Table 1 shows the *k* values and other basic parameters in the von Mises model from the experimental results. The *k* values for the fifteen test data varies from 0.5 to 25 but most of them ranges from 1 to 6. It is interesting to find that, although Qiao et al. [17] improved the electric

accelerated corrosion method by using a pond filled with 3% NaCl solution on the concrete cover surface to obtain the non-uniform corrosion, the k values of corrosion were smaller than 1 and the non-uniformity of rust from the tests were smaller than those from artificial climate environmental tests. The existing experimental data shows that, the non-uniform coefficient can be regarded as a random variable in the range of 1 to 10. In this paper, the randomness of corrosion non-uniformity is considered by Equation (2) and its effect on the reliability will be discussed.

The amount of corrosion products can be expressed as a function of corrosion rate and time as follows [42]:

$$W_{rust} = \sqrt{4\int_0^t 0.105(1/\alpha_{rust})\pi R i_{corr}(t)dt} \tag{3}$$

where α_{rust} is the molecular weight ratio of corrosion products to steel; $i_{corr}(t)$ is the corrosion rate at time t in year.

A corrosion rate model in Chinese National Standard GB/T 51355-2019 [43] which was approved in 2019 was used in this paper. The model was based on numerous experimental and practical data for reinforcement corrosion induced by chloride diffusion, which can be expressed as follows:

$$\ln i_{corr}(t) = 8.617 + 0.618\ln C_{sl} - \frac{3034}{T+273} - 5\times10^{-3}\rho + \ln m_{cl} \tag{4}$$

where C_{sl} is the chloride content at the steel surface (kg/m^3); T is the environmental temperature in (℃). ρ is the resistance of the concrete (kΩ · cm); m_{cl} is the environmental factor in the range of 2~5.5.

The resistance of the concrete can be determined by Zhang's model [44] based on 330 experimental tests as follows:

$$\rho = RH^{-3.68}\left(\frac{t}{28}\right)^{0.3} \times \left\{1.65 + 115\exp\left[-0.259\left(\frac{CE}{100} + 18.4 * \frac{w}{c}\right)\right]\right\}\exp\left[-1.36C_{cl} + 3000\left(\frac{1}{T+273} - \frac{1}{298}\right)\right] \tag{5}$$

where RH is the relative humidity; t is the time (days); CE is the cement content (kg/m^3); w/c is the water/cement ratio; C_{cl} is the chloride content (kg/m^3). In this model, concrete resistance is a function

of relative humidity, time, cement content, chloride content and temperature. It should be mentioned that, the time in this model is from experimental tests within 757 days while this paper considers corrosion propagation time that is normally several decades after construction. Therefore, the time for calculating concrete resistance is simplified as 2 years (i.e., concrete resistance is independent with time after being constructed 2 years).

The chloride content at the steel surface can be determined as follows [43]:

$$C_{sl} = C_{s0} + (C_s - C_{s0})\left[1 - \mathrm{erf}\left(\frac{c \times 10^{-3}}{2\sqrt{D_0 * t}}\right)\right] \quad (6)$$

where C_{s0} is the initial chloride content (kg/m^3). C_s is the surface chloride content (kg/m^3). c is the cover thickness (mm); D_0 is the diffusion coefficient of chloride (m^2/s). t is the time (s).

Current codes for ocean RC structures design (e.g., Hong Kong-Zhuhai-Macau project in China) are mostly based on the prediction of corrosion initiation time because concrete cracking induced by corrosion is challenging to determine [45]. Alternatively, the reliability analysis in this paper focuses on concrete cracking after corrosion initiation, referring to Li and Melchers [26]. Therefore, the C_{s0} in Equation (5) can be taken as the chloride threshold for corrosion initiation. Thus, t in Equation (5) is the time after corrosion initiation. It should be also mentioned that, the accurate prediction of corrosion rate is still challenging although there are many corrosion rate prediction models [46, 47]. This paper just employs the latest model from a Chinese national code [43] which is of practical significance for concrete durability assessment.

Further, the relationship between corrosion degree η and rust amount W_{rust} is given as follows:

$$\eta = \frac{\alpha_{rust} \times W_{rust}}{\rho_{st}\pi R^2} \quad (7)$$

where ρ_{st} is the density of steel.

The above Equations (1)-(7) describe a time-dependent corrosion development considering a stochastic non-uniformity, which will be used for determining concrete cover cracking.

2.2 Meso-scale fracture model for corrosion-induced concrete cracking

To capture the realistic concrete cracking process and accurately predict the concrete cracking mechanism and phenomenon, a meso-scale fracture model of concrete is developed, considering concrete as a three-phase material including aggregates, cement mortar and the interfacial transition zones (ITZ) between aggregates and mortar. For simplification, only coarse aggregates are modelled as polygons with 3-10 sides. Fine aggregates smaller than 2.4 mm and cement are treated as the mortar phase [35]. Coarse aggregates generally occupy 40% of the whole volume of concrete. The size distribution of aggregates follows a typical three-segment grading curve (aggregate size in 2.40–4.76 mm, 4.76–9.52 mm and 9.52–19.05 mm accounting for 20.2%, 39.9% and 39.9%, respectively [48]). The three-phase structure of concrete is produced by an in-house Python script. Aggregates are treated as elastic materials. Zero-thickness cohesive elements are embedded into the mesh of ITZ and mortar to simulate the arbitrary cracking but the material properties of the cohesive elements are defined differently for these two phases. It should be mentioned the measured ITZ thickness normally varies from 10 to 50 μm [49]. The effect of ITZ thickness on corrosion-induced concrete cracking at meso-scale will be discussed in Results Section. More details on the random aggregates generating-packing and insertion process of cohesive elements has been introduced in the authors' previous study [35]. Figure 4 shows the three-phase mesh for RC structure with a reinforcement located at the middle. The RC structure is 150×150 mm and the cover thickness is 40 mm. The diameter of steel bar is 16 mm. The mesh size is 1 mm which is sufficiently fine for simulating concrete cracking in the fracture process zone. There are 15,857 bulk elements and 23,330 zero-thickness cohesive elements in the worked example. The non-uniform corrosion expansion is normally replaced by a displacement boundary for corrosion-induced concrete cracking [11, 18]. Considering the "porous zone" with thickness T_0, the boundary condition based on von Mises model is expressed as follows [4]:

$$T_d(\theta) = \langle (\alpha - 1)\pi R\eta \times \frac{e^{k\cos(\theta-\mu)}}{2\pi I_0(k)} - T_0 \rangle \quad (8)$$

where < > is the Macaulay bracket which ensures $T_d(\theta)$ equals zero if the value in the bracket is smaller than zero, i.e., no corrosion expansion displacement will be applied on concrete if the "porous zone" is not fully filled. In this paper, the "porous zone" thickness is set as a typical value 12.5 μm according to [8, 12, 36]. It should be mentioned the "porous zone" thickness is affected by many factors including concrete strength, water to cement ratio, cover thickness [1]. However, the effect of the variation of "porous zone" thickness is not considered due to the lack of statistic distribution available and limitation of computational capability.

A cohesive law is employed to model the existence of fracture process zone (FPZ) in concrete. Concrete cracking induced by corrosion is a typical tensile-dominated mixed-mode fracture [35]. Thus, the mixed-mode fracture is considered in this study. Before crack initiation, the normal and shear stresses of cohesive elements linearly increase by a slope of penalty stiffness K_p. A mixed-mode fracture criterion is used to determine the crack initiation [35]:

$$\left(\frac{<\sigma_n>}{\sigma_n^0}\right)^2 + \left(\frac{\sigma_s}{\sigma_s^0}\right)^2 = 1 \tag{9}$$

where σ_n and σ_s are the normal and shear stresses of the cohesive elements, respectively; σ_n^0 and σ_s^0 are the tensile and shear strengths of concrete, respectively; $<\sigma_n>$ ensures the normal stress is zero for a compressive state, i.e., compressive stress will not contribute to concrete cracking.

After crack initiation, a damage variable is introduced to control the strain softening which means the normal and shear stress decrease gradually while the corresponding displacement continues to increase. An effective displacement coupling of normal and shear displacements is used to determine the damage variable, which can be expressed as follows [35]:

$$\delta_m = \sqrt{<\delta_n>^2 + {\delta_s}^2} \tag{10}$$

$$D = \frac{\delta_{m,f}\left(\delta_{m,\max} - \delta_{m,0}\right)}{\delta_{m,\max}\left(\delta_{m,f} - \delta_{m,0}\right)} \tag{11}$$

where δ_m is the effective displacement or separation in the mixed-mode plane; δ_n and δ_s are the normal and shear displacements in the normal and shear planes, respectively. $\delta_{m,0}$ is the critical effective displacement to crack initiation. $\delta_{m,\max}$ is the historical maximum effective displacement. $\delta_{m,f}$ is the effective failure displacement for the damage value reaching unity, which can be determined by a B-K criterion with fracture energies for Mode I, Mode II and mixed ratio [35].

2.3 Machine Learning-Based Surrogate Modelling

The problem to be tackled is the prediction of critical corrosion degree corresponding to different instantaneous crack widths for a given non-uniform coefficient, using the data produced by 90 meso-scale numerical simulation. This is a typical supervised machine learning problem, in particular, a machine learning regression. An input space $\mathbf{X} \in \mathbb{R}^d$ composed of d input features (in this paper there is only one input feature), an output space $\mathbf{Y} \in \mathbb{R}^D$ composed of D output features (in this paper there are four output features), and a dataset with n examples, i.e., input/output relation $\mathbf{D}_n = \left\{\left(x_1, y_1^{\mathrm{I}}, y_1^{\mathrm{II}}, y_1^{\mathrm{III}}, y_1^{\mathrm{IV}}\right), \cdots, \left(x_n, y_n^{\mathrm{I}}, y_n^{\mathrm{II}}, y_n^{\mathrm{III}}, y_n^{\mathrm{IV}}\right)\right\}$. In short, the scope is to learn the input/output relation $\mu: \mathbf{X} \rightarrow \mathbf{Y}$ merely based on $\mathbf{D}_n$**.** This paper exploits the artificial neural network algorithm to develop a surrogate model which approximates the input/output relation. Neural Networks are a family of techniques which systematically combine simple approximations of a human brain neuron, called perceptron, to build a complex network [50]. The neurons are organised in stacked layers connected by weights and bias that are learned based on the available data via backpropagation [51]. It is called a shallow neural network if the architecture only consists of one hidden layer. Conversely, it is called a deep neural network if the architecture consists of multiple hidden layers. In the present problem where the number of samples are limited, it is more reasonable to employ a shallow architecture . The entire database is divided into training subset (70%), validation subset (15%) and testing subset (15%). The validation subset is used to validate that the network is generalizing and to stop training before overfitting. The testing subset is to independently examine network generalization. The model is trained using the Levenberg-Marquardt method [52]. This algorithm appears to be the fastest method

for training moderate-sized feedforward neural networks. The training stops until the mean square error of the validation data subset increases consecutively for six iterations.

2.4 Reliability Analysis

In the process of determining the probability of failure and reliability of a system, a limit state equation must be written first. This is formulated by the stochastic variables that determines whether the system will fail or not. In the present reliability analysis, the limit state is defined as the instantaneous crack width exceeding a prescribed critical value, which can be expressed as follows.

$$g(t) = W(t,k) - W_{cr} \tag{12}$$

where $g(t)$ is the time-dependent safety margin; $W(t,k)$ is the instantaneous crack width as a function of time for non-uniform corrosion coefficient k; W_{cr} is the critical crack width. The effects of different critical crack width prescribed in the limit state equation will be discussed later. Correction factors may also be considered for both $W(t,k)$ and W_{cr} to accommodate the aleatoric and epistemic uncertainties. For simplicity, these are ignored in the present study. If $g(t)$ is larger than zero, the system is in the safe domain. If $g(t)$ is smaller than zero, the system is in the failed domain. If $g(t)$ is equal to zero, the system is at the limit state, but this is still regarded as failure.

As a machine learning-based surrogate model is employed to evaluate the instantaneous crack width, the formulated limit state equation is an implicit one. Direct evaluation of probability of failure may be impractical. Alternatively, the probability of failure (P_f) at each time instance is approximated by a Monte Carlo Sampling as follows:

$$P_f = P(W - W_{cr} \leq 0) \approx \frac{n_f}{N} \tag{13}$$

where n_f is the number of failure observed and N is the total number of sampling. The Monte Carlo Simulation must be stopped at some points. Unfortunately, it is extremely difficult to know with great confidence at which the number of simulations is enough to guarantee sufficient accuracy. A common approach is to plot the estimated probability of failure against the number of simulations. This should show the estimated probability of failure progressively converging to the actual value as the number

of simulations increase [53]. Alternative measure is the coefficient of variation (COV) of the predicted probability of failure as follows:

$$cov(P_f) \approx \frac{\sqrt{\frac{(1-P_f)P_f}{N}}}{P_f} \tag{14}$$

This approach assumes that each simulation can be treated as a Bernoulli trial, and that the number of failures should follow the binomial distribution [54]. Note that "N" in Equation (15) indicates the number of completed trials. The effect of different numbers of Monte Carlos sampling will be elaborated in the following sections.

3. RESULTS

3.1 Concrete cracking

A uniform distribution of non-uniform corrosion coefficient k in the range of 0 to 10 and the corresponding crack width will be used as a database for machine learning. All the basic mechanical parameters in the concrete fracture model and corrosion rate model are listed in Table 2. Figure 5 shows four cases of crack patterns of concrete induced by corrosion for non-uniform coefficient values 0.26, 1.28, 3.28 and 5.94. It can be seen that, the crack patterns are significantly affected by the non-uniform coefficient. For a small value of k, more cracks are produced around the reinforcement. For a large value of k, two side cracks are formed to make concrete cover delaminate. Concrete surface cracking at the location nearest steel bar and microcracks in the ITZs dominate the crack pattern. Therefore, due to the nature of heterogeneity, concrete cracking involves some complex toughing mechanisms (e.g., aggregate bridging, microcrack shielding) at meso-scale. Simplified analytical method or homogeneous numerical method with a modified stress-strain softening model cannot accurately predict the crack patterns and crack width for reinforced concrete.

Figure 6a illustrates the surface crack width of concrete as a function of time for four k values including uniform corrosion and non-uniform corrosion. It can be found that, concrete surface cracking for uniform corrosion occurs later than that for non-uniform corrosion and a larger k value

leads to earlier concrete surface cracking. With the corrosion develops, the surface crack width continues to increase. The growth of surface crack width for k=0 (i.e., uniform corrosion) is slightly faster than that for k=1.28. This is because the inner cracks in concrete for k=1.28 release the stress concentration on the top cover and postpone the surface crack development. For the same corrosion time 5 years, the crack width for uniform corrosion k=0 is only 0.11 mm while that for k=5.94 is about 0.23 mm. Therefore, the non-uniformity significantly affects corrosion-induced concrete cracking patterns and crack width development. Figure 6b shows the surface crack width development affected by ITZ thickness. It can be seen that the crack width developments for ITZ thickness 0-50 μm are almost the same. This is because corrosion-induced concrete cracking is dominated by tensile fracture while the deformation or strain of the very thin ITZ before crack initiation can be ignored. Therefore, zero-thickness cohesive elements can be practically used for mortar and ITZ cracking.

Crack width is an important parameter for the serviceability of RC structures because cracks can significantly accelerate the corrosion process of reinforcement and weaken the bond performance between reinforcement and concrete cover. American Concrete Institute (ACI) [24] presented acceptable crack widths for different service conditions, e.g., 0.15 mm and 0.3 mm for the exposure conditions of seawater and moist air, respectively. It should be mentioned that this code is for the purpose of controlling concrete crack under loadings while it can also be used as a guidance for allowable crack widths induced by corrosion [26, 55]. Therefore, we investigate the effect of non-uniform coefficient on critical corrosion degrees to different critical crack widths. Figure 7 illustrates the corrosion degrees to crack widths reaching 0.1, 0.15, 0.2, 0.3 mm for the non-uniform corrosion coefficient k varying 0 to 10. It should be mentioned that, some values of corrosion degrees to crack width 0.2 and 0.3 mm are missing due to numerical simulations are unable to convergence with crack width increasing. It is apparent that if k is greater than 2, a smaller corrosion degree is needed for reaching critical crack widths for a larger k value. In contrast, if k is in the range of 0 to 2, the non-uniformity has little effect on the critical degrees for crack width reaching 0.1 mm and 0.15 mm. However, with a smaller k, the critical degrees to crack width reaching 0.2 mm and 0.3 mm are smaller.

Thus, $k = 2$ seems to be a crucial threshold. As discussed above, this is because the inner cracks for k around 1-2 postpone the surface crack development. Moreover, the effect of non-uniformity becomes more significant as the critical crack width increases. This is because the non-uniform corrosion coefficient changes the crack patterns which further affect the surface crack width development. Thus, the assessment of RC structures serviceability should consider the non-uniform corrosion of the reinforcement.

3.2 Verification of crack width

To verify the developed numerical method, numerical results on crack width are compared with experimental results from Andrade [56]. The concrete cover is 20 mm and a steel bar with a dimeter of 16 mm is placed in the middle of the concrete beam. The tests employed electric current method to accelerate reinforcement corrosion so uniform corrosion (k=0) is used for the corrosion boundary condition in the numerical model. All the basic parameters in the numerical model are given in Table 3. The corrosion expansion displacement is expressed as a function of steel radius loss as follows:

$$T_d = (\alpha - 1) \times \Delta R - T_0 \tag{15}$$

where ΔR is the radius loss of rebar.

To consider the effect of aggregate randomness on the crack width developments, 10 random meso-scale concrete with the coarse aggregate fraction 40% are modelled. Figure 8a shows the crack width developments obtained from numerical and experimental results. It can be seen that, the effect of aggregates randomness on the crack width development is limited, which proves the repeatability of the developed numerical method. The progress of crack width simulated is in reasonably good agreement with the experimental results [56]. It should be mentioned that the electric corrosion method perhaps caused more severe corrosion in the middle of the beam which made crack width at the middle of specimen larger than that at both sides. Our numerical method assumes the corrosion-induced concrete cracking as a two-dimensional plain strain problem, which makes the simulated crack width slightly larger than the crack width from the experiment.

Further, experimental results for crack width development induced by non-uniform corrosion from Ye et al. [57] are collected to verify the developed numerical method. The thickness values of rust layer for specimen C15 in [57] are obtained and fitted into the von Mises model (i.e., Equation 1). The determined non-uniform coefficient k is 1.6. A numerical model with the same dimensions of specimen C15 is developed. All the basic mechanical parameters are given in Table 3. Figure 8b illustrates the crack width development as a function of corrosion degree from numerical and experimental results. It can be seen the numerical result has a good agreement with the experimental data. The comparison between the numerical and experimental results for uniform and non-uniform corrosion demonstrates that the developed numerical method is capable of predicting corrosion-induced crack width development.

3.3 Surrogate models

A shallow neural network model with three neurons in the hidden layer is developed to predict the corrosion degrees corresponding to instantaneous crack width of 0.1 mm, 0.15 mm, 0.2 mm and 0.3 mm, for a given non-uniform coefficient (k). Correlation plots of the actual data and predicted values are shown in Figure 9. The surrogate model achieves a remarkably good performance with coefficients of determination (R^2) in all datasets close to unity. With the achieved prediction accuracy, the surrogate model should be suitable for the incorporation with reliability analysis. In the meantime, any prediction made by the developed surrogate model can be completed within seconds, as compared with up to 48 hours CPU time per simulation if the meso-scale model is adopted. This immediately shows the importance of developing data-driven surrogate model for this study.

3.4 Time-dependent probability of failure

Typical estimation of time-dependent probability of failure is presented in Figure 10a. The critical crack width is prescribed as W_{cr}=0.3 mm, which is a common specification in state-of-the-art design code [24]. The Monte Carlo Simulation is performed with half-year as an increment. The initial failure is observed approximately after 6 years. It should be noted that the time here corresponds to the period

after corrosion initiation. To elucidate the effect of sampling number of Monte Carlo Simulation, a comparison is made for several sampling numbers (N = 100, 1000, 2000 and 5000). The running plots showing the progressive relation between probability of failure, COV of probability of failure versus the sampling number are given in Figures 10b and 10c, respectively. It can be observed that the predicted probability of failure and its COV, for instance at 10, 12.5 and 15 years, fluctuates in the initial phase of sampling and converges to a reasonable degree when N > 2000. As the variations shown in Figures 10c are seemingly small, the sampling number N = 2000 is thus selected for the comparative analysis in the following section.

4. DISCUSSION

4.1 Effect of corrosion model

As reviewed in the previous section, the non-uniform corrosion has a great impact on the concrete cracking. This also motivates the development of a non-uniform corrosion model. Whist the corrosion model adopted in this paper is devised to deal with the non-uniform corrosion, it is also able to handle uniform corrosion by assuming k = 0. Figure 11 shows the comparison of time-dependent probability of failure predicted by uniform and non-uniform corrosion model. In this comparison, the critical crack width is prescribed as 0.3 mm. Regarding the evaluation based on uniform corrosion model, the randomness entirely comes from the corrosion rate. As for the non-uniform corrosion model, the sampling of k is driven by the three-parameter log-logistic distribution, and a normal distribution based on the same database. If the non-uniform coefficient k is considered as a random variable, the limit state violation in the samples can be observed after 5 years of corrosion initiation. However, the increasing rate of the probability of failure is smaller than that of the uniform corrosion. This is mainly because most of the samples of k are in the range of 2 to 4, in which case the failure would occur after 12 years. If the acceptable level of risk is assumed to $P_f = 0.2$ [55], the remaining serviceable lives are 9.4 years, 8.3 years, and 13.9 years, if the non-uniform corrosion model with log-logistic distribution of k, non-uniform corrosion model with normal distribution of k and uniform corrosion

model are adopted respectively. For non-uniform corrosion, the safe service life after corrosion initiation is shortened by about 32% than that for uniform corrosion. Thus, the assumption of uniform corrosion over-predicts the remaining serviceability of reinforced concrete structures, which also highlights the importance of using non-uniform corrosion in the safety design for critical buildings and infrastructures.

4.2 Effect of critical crack width

The critical crack width prescribed in the limit state equation is an important parameter for the reliability analysis. Previous section shows the time-dependent probability of failure assuming W_{cr}=0.3 mm. The comparison of time-dependent probability of failure for different critical crack widths prescribed in the limit state equation is shown in Figure 12. With a smaller critical crack width prescribed in the limit state equation, the initial limit state violation in the samples can be observed earlier. For instance, the first limit state violation in the sample can be observed after 1 year, 1.5 years, 2.5 years and 4.5 years, for the critical crack width 0.1, 0.15, 0.2 and 0.3 mm, respectively. The increase rate of the probability of failure with time differs between different prescribed critical crack widths, i.e., if the prescribed critical crack width is smaller, the increasing rate would be larger. This is mainly due to the smaller difference of the critical corrosion degree between different non-uniform coefficient specification (i.e., k). Since there is little difference in the critical corrosion degree between different non-uniform coefficient samples, the probability of failure would approach unity rapidly.

4.3 Effect of environmental parameters

A comparison of time-dependent probability of failure based on environmental parameters (surface chloride content, temperature and relative humidity) is given in Figure 13. In this comparison, the critical crack width is assumed as 0.3 mm. The latest durability standard GB/T 51355-2019 [43] listed the suggested values for surface chloride content in China's costal atmosphere zones, i.e., 5.87

kg/m^3(distance <0.1 km), 3.83 kg/m^3(0.1 km < distance < 0.25 km), 2.57 kg/m3(0.25 km < distance < 0.5 km) and 1.28 kg/m^3(0.5 km < distance < 1 km). It can be seen from Figure 13a that, an increase of surface chloride content from 1.28 to 5.87 can lead to a reduction of the remaining serviceable time from 11.5 years to 7.3 year, assuming that the acceptable level of risk is $P_f = 0.2$. Therefore, for costal structures, the residual service life after corrosion initiation is significantly affected by the distance between structures and coastline. Figure 13b illustrates the time-dependent probability of failure for different environmental temperatures. It can be seen that, the failure probability is closed related to the temperature and the higher the temperature is, the failure is earlier to occur. The increasing rate of failure probability is also larger for a higher temperature. If the average annual temperature is increased by 5 ℃ from 20 ℃ to 25 ℃, the remaining serviceable time after corrosion initiation can be reduced by 30% from 13.5 years to 9.4 years, assuming that the acceptable level of risk $P_f = 0.2$. Therefore, it can be predicted that global warming would have a significant impact on structural serviceability life. Figure 13c shows the time-dependent probability of failure for different environmental relative humidity values. It can be found that, the larger the humidity is, the failure is earlier to occur and the increasing rate of failure probability is larger. Assuming the acceptable level of risk $P_f = 0.2$, the increase of relative humidity from 65% to 95% can lead to a reduction of the remaining serviceable time from 12.4 years to 8.5 years.

A sensitivity analysis is carried out to investigate the environmental parameters that influence the failure probability. Figure 14 illustrates the sensitivity analysis of cracking failure time to the environmental parameters. The failure time is based on the acceptable level of risk $P_f = 0.2$. It can be seen that, with the increasing of surface chloride content, temperature and relative humidity, the failure time is close to linearly decreasing. Moreover, the failure time is most sensitive to temperature, followed by relative humidity and surface chloride content. It should be mentioned that, the temperature and relative humidity used in this paper are simplified as the external environmental

parameters. It is worthy to monitor and determine the internal temperature and relative humidity in the concrete cover to determine a more accurate corrosion rate.

Reliability analysis of non-uniform corrosion induced concrete cracking presented in this paper shows that the non-uniformity significantly affects the corrosion-induced concrete cracking. The assumption of uniform corrosion over-predicts the remaining safe life of reinforced concrete structures. For non-uniform corrosion, the safe service life after corrosion initiation is shorten by about 32% than that for uniform corrosion. It is of practical significance to use non-uniform corrosion in the safety design and repair decisions for critical buildings and infrastructures.

Given the meso-scale modelling of corrosion-induced concrete cracking is very time-consuming and the proposed machine-learning method requires lots of data for training, the effects of concrete strength, cover thickness, reinforcement diameter, "porous zone" thickness between reinforcement and concrete on reliability are not considered in this paper. Future work will be carried out to cover more variables and improve numerical efficiency.

5. CONCLUSIONS

A machine-learning based time-dependent reliability analysis for non-uniform corrosion-induced cracking of reinforced concrete structures is presented in this paper. A stochastic non-uniform corrosion model and a corrosion rate model are combined with the advanced meso-scale numerical modelling for predicting the crack growth in concrete. The developed model is verified with experimental results on the crack width development. Monte Carlo Simulation is performed and a number of crucial influencing factors including the effects of critical crack width, corrosion model and corrosion rate are investigated. It has been found that, the non-uniformity of corrosion significantly affects corrosion-induced concrete cracking and its effect becomes more significant as the critical crack width increases. For non-uniform corrosion, the safe service life after corrosion initiation is shorten by about 32% than that for uniform corrosion. With the increasing of surface

chloride content, temperature and relative humidity, the failure time is linearly decreased. Moreover, the predicted failure probability is most sensitive to temperature, followed by relative humidity and surface chloride content. The analysis results demonstrate the significance of considering the non-uniformity of corrosion of reinforcement and its effect on the time-dependent reliability. As compared to the traditional uniform assumption, the present approach can yield a safer and more reliable design approach.

ACKNOWLEDGEMENT

Financial support from the UK Engineering and Physical Sciences Research Council (EP/S005560/1; EP/W027763/1) is thankfully acknowledged.

REFERENCES

[1] F. Chen, C.-Q. Li, H. Baji, B. Ma, Effect of design parameters on microstructure of steel-concrete interface in reinforced concrete, Cem. Concr. Res. 119 (2019) 1-10.
[2] X. Gu, H. Guo, B. Zhou, W. Zhang, C. Jiang, Corrosion non-uniformity of steel bars and reliability of corroded RC beams, Eng. Struct. 167 (2018) 188-202.
[3] H.S. Wong, Y.X. Zhao, A.R. Karimi, N.R. Buenfeld, W.L. Jin, On the penetration of corrosion products from reinforcing steel into concrete due to chloride-induced corrosion, Corros. Sci. 52(7) (2010) 2469-2480.
[4] X. Xi, S. Yang, C.-Q. Li, A non-uniform corrosion model and meso-scale fracture modelling of concrete, Cement and Concrete Research 108 (2018) 87-102.
[5] U.M. Angst, Challenges and opportunities in corrosion of steel in concrete, Mater. Struct. 51(1) (2018).
[6] K. Vu, M.G. Stewart, J. Mullard, Corrosion-induced cracking: Experimental data and predictive models, ACI Structural Journal 102(5) (2005) 719-726.
[7] J.A. Mullard, M.G. Stewart, Corrosion-induced cover cracking: new test data and predictive models, ACI Structural Journal 108(1) (2011) 71-79.
[8] C.Q. Li, R.E. Melchers, J.J. Zheng, Analytical model for corrosion-induced crack width in reinforced concrete structures, ACI Structural Journal 103(4) (2006) 479-487.
[9] C.Q. Li, S.T. Yang, Prediction of concrete crack width under combined reinforcement corrosion and applied load, J. Eng. Mech. 137(11) (2011) 722-731.
[10] P. Grassl, T. Davies, Lattice modelling of corrosion induced cracking and bond in reinforced concrete, Cement and Concrete Composites 33(9) (2011) 918-924.
[11] B. Šavija, M. Luković, J. Pacheco, E. Schlangen, Cracking of the concrete cover due to reinforcement corrosion: A two-dimensional lattice model study, Constr. Build. Mater. 44 (2013) 626-638.
[12] A. Jamali, U. Angst, B. Adey, B. Elsener, Modeling of corrosion-induced concrete cover cracking: A critical analysis, Constr. Build. Mater. 42 (2013) 225-237.
[13] C. Fu, N. Jin, H. Ye, X. Jin, W. Dai, Corrosion characteristics of a 4-year naturally corroded reinforced concrete beam with load-induced transverse cracks, Corros. Sci. 117 (2017) 11-23.
[14] R.E. Melchers, C.Q. Li, M.A. Davison, Observations and analysis of a 63-year-old reinforced concrete promenade railing exposed to the North Sea, Mag. Concrete. Res. 61(4) (2009) 233-243.
[15] Y. Yuan, Y. Ji, Modeling corroded section configuration of steel bar in concrete structure, Constr. Build. Mater. 23(6) (2009) 2461-2466.

[16] Y. Zhao, A.R. Karimi, H.S. Wong, B. Hu, N.R. Buenfeld, W. Jin, Comparison of uniform and non-uniform corrosion induced damage in reinforced concrete based on a Gaussian description of the corrosion layer, Corros. Sci. 53(9) (2011) 2803-2814.
[17] D. Qiao, H. Nakamura, Y. Yamamoto, T. Miura, Crack patterns of concrete with a single rebar subjected to non-uniform and localized corrosion, Constr. Build. Mater. 116 (2016) 366-377.
[18] J. Chen, W. Zhang, Z. Tang, Q. Huang, Experimental and numerical investigation of chloride-induced reinforcement corrosion and mortar cover cracking, Cem. Concr. Compos. 111 (2020).
[19] Y. Zhao, B. Hu, J. Yu, W. Jin, Non-uniform distribution of rust layer around steel bar in concrete, Corros. Sci. 53(12) (2011) 4300-4308.
[20] X. Xi, S. Yang, Investigating the spatial development of corrosion of corner-located steel bar in concrete by X-ray computed tomography, Constr. Build. Mater. 221 (2019) 177-189.
[21] S. Yang, X. Xi, K. Li, C.-Q. Li, Numerical Modeling of Nonuniform Corrosion-Induced Concrete Crack Width, J. Struct. Eng. 144(8) (2018) 04018120.
[22] Y. Zhao, J. Yu, B. Hu, W. Jin, Crack shape and rust distribution in corrosion-induced cracking concrete, Corros. Sci. 55 (2012) 385-393.
[23] E. Chen, C.K.Y. Leung, Finite element modeling of concrete cover cracking due to non-uniform steel corrosion, Eng. Fract. Mech. 134 (2015) 61-78.
[24] A.C.I. Committee, 224R-01: Control of Cracking in Concrete Structures (Reapproved 2008), Technical Documents (2008).
[25] f. 2010, fib Model Code for Concrete Structures 2010, 2013.
[26] C.Q. Li, R.E. Melchers, Time-Dependent Reliability Analysis of Corrosion-Induced Concrete Cracking, ACI STRUCTURAL JOURNAL 102(4) (2005) 105-116.
[27] K.A.T. Vu, M.G. Stewart, Structural reliability of concrete bridges including improved chloride-induced corrosion models, Struct. Saf. 22(4) (2000) 313-333.
[28] K. Zhang, J. Xiao, Time-dependent reliability analysis on carbonation behavior of recycled aggregate concrete based on gamma process, Constr. Build. Mater. 158 (2018) 378-388.
[29] K. Zhang, J. Xiao, Prediction model of carbonation depth for recycled aggregate concrete, Cem. Concr. Compos. 88 (2018) 86-99.
[30] K. Zhang, J. Xiao, Y. Zhao, Q. Zhang, Analytical model for critical corrosion level of reinforcements to cause the cracking of concrete cover, Constr. Build. Mater. 223 (2019) 185-197.
[31] F. Biondini, D.M. Frangopol, Lifetime reliability-based optimization of reinforced concrete cross-sections under corrosion, Struct. Saf. 31(6) (2009) 483-489.
[32] V. Val Dimitri, Deterioration of Strength of RC Beams due to Corrosion and Its Influence on Beam Reliability, J. Struct. Eng. 133(9) (2007) 1297-1306.
[33] M. Zhang, M. Akiyama, M. Shintani, J. Xin, D.M. Frangopol, Probabilistic estimation of flexural loading capacity of existing RC structures based on observational corrosion-induced crack width distribution using machine learning, Struct. Saf. 91 (2021).
[34] K. Zhang, J. Xiao, Q. Zhang, Time-dependent reliability analysis of recycled aggregate concrete cover cracking induced by reinforcement corrosion, Journal of Building Engineering 39 (2021) 102320.
[35] X. Xi, S. Yang, C.-Q. Li, M. Cai, X. Hu, Z.K. Shipton, Meso-scale mixed-mode fracture modelling of reinforced concrete structures subjected to non-uniform corrosion, Eng. Fract. Mech. 199 (2018) 114-130.
[36] X. Du, L. Jin, R. Zhang, Modeling the cracking of cover concrete due to non-uniform corrosion of reinforcement, Corros. Sci. 89 (2014) 189-202.
[37] Y. Zhao, X. Xu, Y. Wang, J. Dong, Characteristics of pitting corrosion in an existing reinforced concrete beam exposed to marine environment, Constr. Build. Mater. 234 (2020) 117392.
[38] D.J. Best, N.I. Fisher, Efficient Simulation of the von Mises Distribution, Journal of the Royal Statistical Society. Series C (Applied Statistics) 28(2) (1979) 152-157.
[39] B.S. Jang, B.H. Oh, Effects of non-uniform corrosion on the cracking and service life of reinforced concrete structures, Cem. Concr. Res. 40(9) (2010) 1441-1450.
[40] T. Pan, Y. Lu, Stochastic Modeling of Reinforced Concrete Cracking due to Nonuniform Corrosion: FEM-Based Cross-Scale Analysis, J. Mater. Civ. Eng. 24(6) (2012) 698-706.

[41] J. Chen, W. Zhang, X. Gu, Modeling time-dependent circumferential non-uniform corrosion of steel bars in concrete considering corrosion-induced cracking effects, Eng. Struct. 201 (2019).
[42] Y. Liu, R.E. Weyers, Modelling the time-to-corrosion cracking in chloride contaminated reinforced concrete structures, ACI Mater. J. 95(6) (1998) 675-681.
[43] D. Niu, S. Wang, Y. Hui, F. Xing, Standard for Durability Assessment of Existing Concrete Structures (GB/T 51355-2019), Beijing, 2019.
[44] Q. Zhang, P.-Y. Lun, X. Li, A simplified approach for prediction of concrete resistivity: experimental study and mathematic model, Mater. Struct. 54(4) (2021).
[45] K. Li, D. Zhang, Q. Li, Z. Fan, Durability for concrete structures in marine environments of HZM project: Design, assessment and beyond, Cem. Concr. Res. 115 (2019) 545-558.
[46] Z.-H. Lu, P.-Y. Lun, W. Li, Z. Luo, Y. Li, P. Liu, Empirical model of corrosion rate for steel reinforced concrete structures in chloride-laden environments, Adv. Struct. Eng 22(1) (2018) 223-239.
[47] P.-Y. Lun, Z.-H. Lu, X.-g. Zhang, Q. Zhang, R. Zhao, Experimental study and suggested mathematical model for chloride-induced reinforcement corrosion rate, Structures 34 (2021) 2014-2029.
[48] A.M. Neville, Properties of concrete, Fourth ed., Pearson Education Limited, London, 2006.
[49] J. Xiao, W. Li, D.J. Corr, S.P. Shah, Effects of interfacial transition zones on the stress–strain behavior of modeled recycled aggregate concrete, Cem. Concr. Res. 52 (2013) 82-99.
[50] F. Rosenblatt, The perceptron: a probabilistic model for information storage and organization in the brain, Psychological review 65(6) (1958).
[51] D.E. Rumelhart, G.E. Hinton, R.J. Williams, Learning representations by back-propagating errors, Nature 323(6088) (1986) 533-536.
[52] D.W. Marquardt, An Algorithm for Least-Squares Estimation of Nonlinear Parameters, Journal of the Society for Industrial and Applied Mathematics 11(2) (1963) 431-441.
[53] R.E. Melchers, A.T. Beck, Structural Reliability Analysis and Prediction, Wiley2018.
[54] A. Haldar, S. Mahadevan, Reliability Assessment Using Stochastic Finite Element Analysis, Wiley2000.
[55] H. Baji, C.-Q. Li, S. Scicluna, J. Dauth, Risk-cost optimised maintenance strategy for tunnel structures, Tunnel. Underground Space Technol. 69 (2017) 72-84.
[56] C. Andrade, F.J. Molina, C. Alonso, Cover cracking as a function of rebar corrosion: Part 1-experiment test, Mater. Struct. 26 (1993) 453-454.
[57] H. Ye, N. Jin, C. Fu, X. Jin, Rust distribution and corrosion-induced cracking patterns of corner-located rebar in concrete cover, Constr. Build. Mater. 156 (2017) 684-691.
[58] Y. Yuan, Y. Ji, Y. Mu, Propagation and model of distribution for corrosion of steel bars in concrete, China Civil Engineering Journal 40(7) (2007).
[59] W. Ren, Z. Yang, R. Sharma, C. Zhang, P.J. Withers, Two-dimensional X-ray CT image based meso-scale fracture modelling of concrete, Eng. Fract. Mech. 133 (2015) 24-39.

Table 1 The k values and other parameters formulated in the von Mises corrosion model

Data resource	η	k	μ	R^2	Steel bar location	Accelerate corrosion method
Yuan et al. [15, 58]	0.19%	3.122	3.181	0.99	Middle	Artificial climate environment
	0.56%	0.555	3.188	0.93	Middle	
	0.12%	1.832	3.325	0.93	Middle	
Zhao et al. [19]	0.18%	3.285	3.173	0.90	Corner	Wetting and drying cycles
	0.18%	3.232	3.182	0.91	Corner	
	0.18%	3.285	3.173	0.90	Middle	
Qiao et al. [17]	0.42%	0.923	2.963	0.95	Middle	Improved electric corrosion
	0.81%	0.689	3.540	0.77	Middle	
Chen et al. [18]	0.018%	25.28	3.170	0.79	Middle	Marine atmosphere environment
	0.08%	5.878	3.090	0.86	Middle	
	0.13%	4.176	3.174	0.91	Middle	
	0.19%	3.210	3.150	0.95	Middle	
	0.13%	1.805	3.180	0.89	Corner	
	0.26%	1.197	3.190	0.87	Corner	
	0.32%	1.043	3.140	0.85	Corner	

Table 2 All the basic parameters in the fracture model and corrosion rate model [35, 43]

Description	Values	Description	Values
Young's modulus of aggregate	70 GPa	Shear strength of mortar	5.2 MPa
Young's modulus of mortar	25 GPa	Shear strength of ITZ	2.6 MPa
Poisson's ratio of aggregate	0.2	Mode I fracture energy of mortar	40 N/m
Poisson's ratio of mortar	0.2	Mode I fracture energy of ITZ	17 N/m
Tensile strength of mortar	2.6 MPa	Mode II fracture energy of mortar	80 N/m
Tensile strength of ITZ	1.3 MPa	Mode II fracture energy of ITZ	34 N/m
Surface chloride content	2.57 kg/m^3	Chloride threshold	0.748 kg/m^3
Diffusion coefficient	6×10^{-12} m^2/s	Temperature	25 °C
Relative humidity	85%	Environmental factor	4.5
Cement content	350 kg/m^3	Water/cement ratio	0.4

Table 3 Values used for comparison and validation [35, 56, 57, 59]

	Description	Values	Description	Values
Uniform corrosion k=0	Young's modulus of aggregate	70 GPa	Cohesive strength of mortar	6 MPa
	Young's modulus of mortar	25 GPa	Cohesive strength of ITZ	2 MPa
	Poisson's ratio of aggregate	0.2	Fracture energy of mortar	60 N/m
	Poisson's ratio of mortar	0.2	Fracture energy of ITZ	30 N/m
Non-uniform corrosion k=1.6	Young's modulus of aggregate	70 GPa	Cohesive strength of mortar	8 MPa
	Young's modulus of mortar	35 GPa	Cohesive strength of ITZ	3 MPa
	Poisson's ratio of aggregate	0.2	Fracture energy of mortar	80 N/m
	Poisson's ratio of mortar	0.2	Fracture energy of ITZ	45 N/m

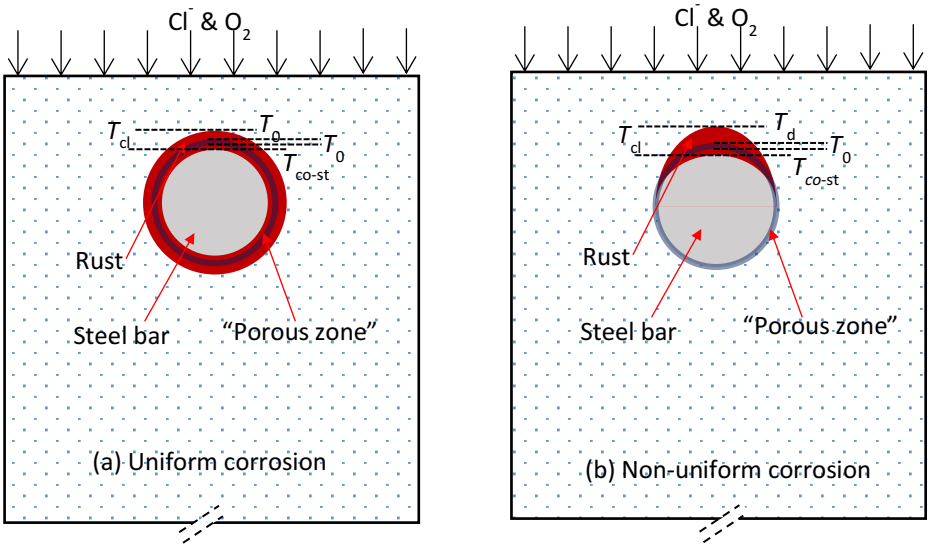

Figure 1 Corrosion of reinforcement in concrete: (a) uniform corrosion; (b) non-uniform corrosion. T_{cl} is the total thickness of rust which can be divided into three parts: $T_{co\text{-}st}$ - the corroded/loss thickness of steel bar; T_0 - rust filling into the "porous zone" between concrete and steel bar; T_d - rust expanding out of original steel bar to crack concrete.

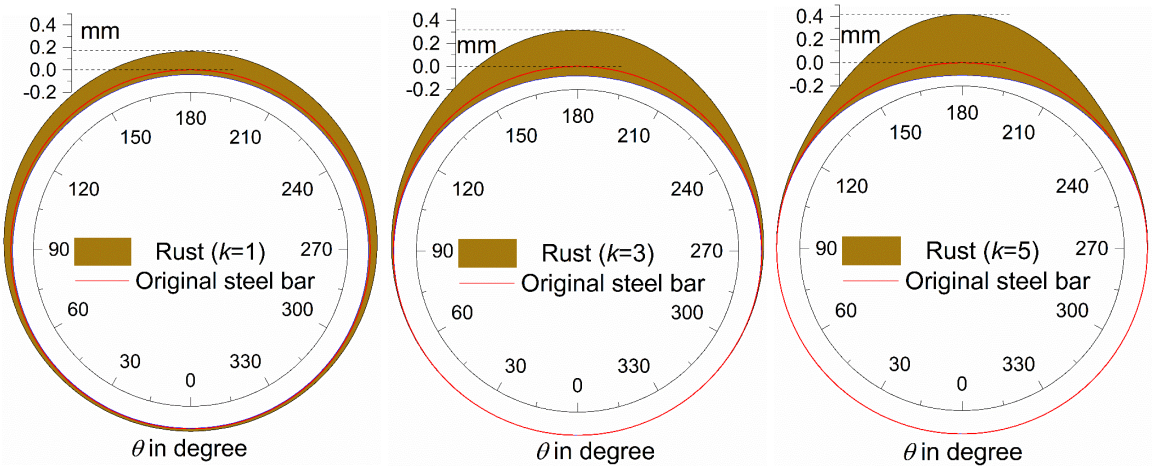

(a) (b) (c)

Figure 2 Rust distribution of von Mises corrosion model for: (a) k=1; (b) k=3; (c) k=5. The parameters in Equation (1) are: α=3.83; R=8 mm; η=0.5%; μ=180°. The rust thickness T_{cl} is scaled by 5 times for clearly showing.

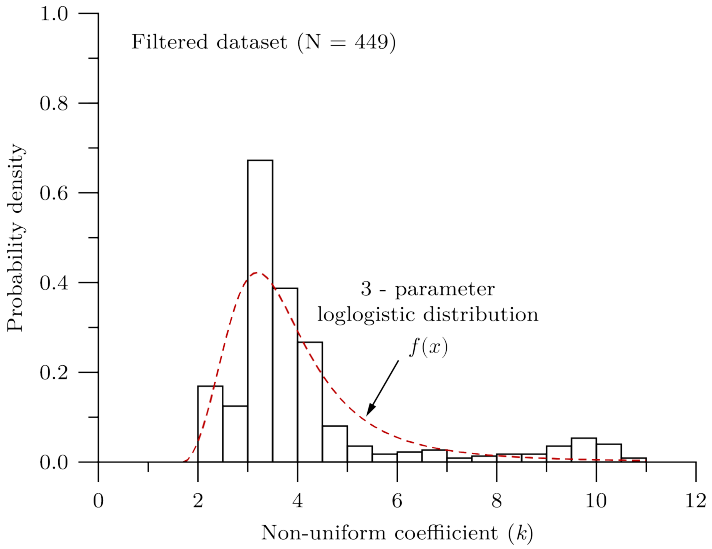

675

676 Figure 3 Probability density of non-uniform corrosion coefficient k

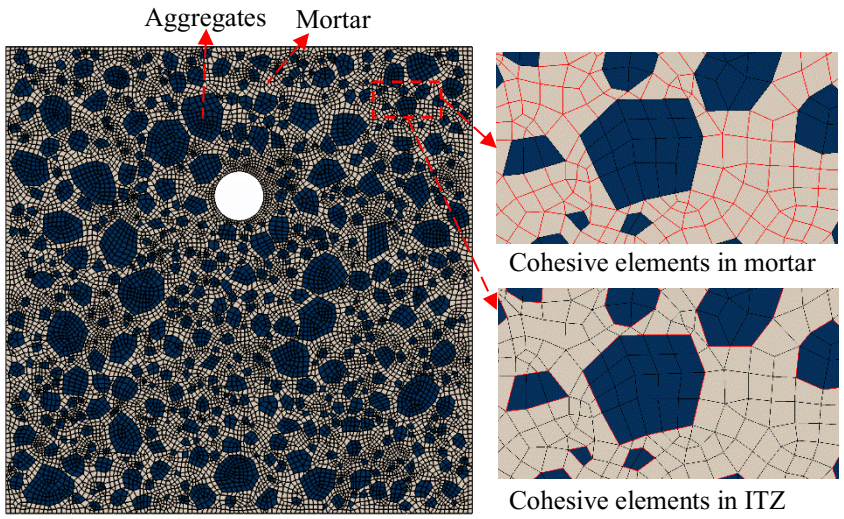

677

678 Figure 4 Meso-scale concrete fracture model with cohesive elements. The mesh size is 1 mm. Zero-
679 thickness cohesive elements are inserted into meshes of mortar and ITZ for arbitrary cracking.

680
681

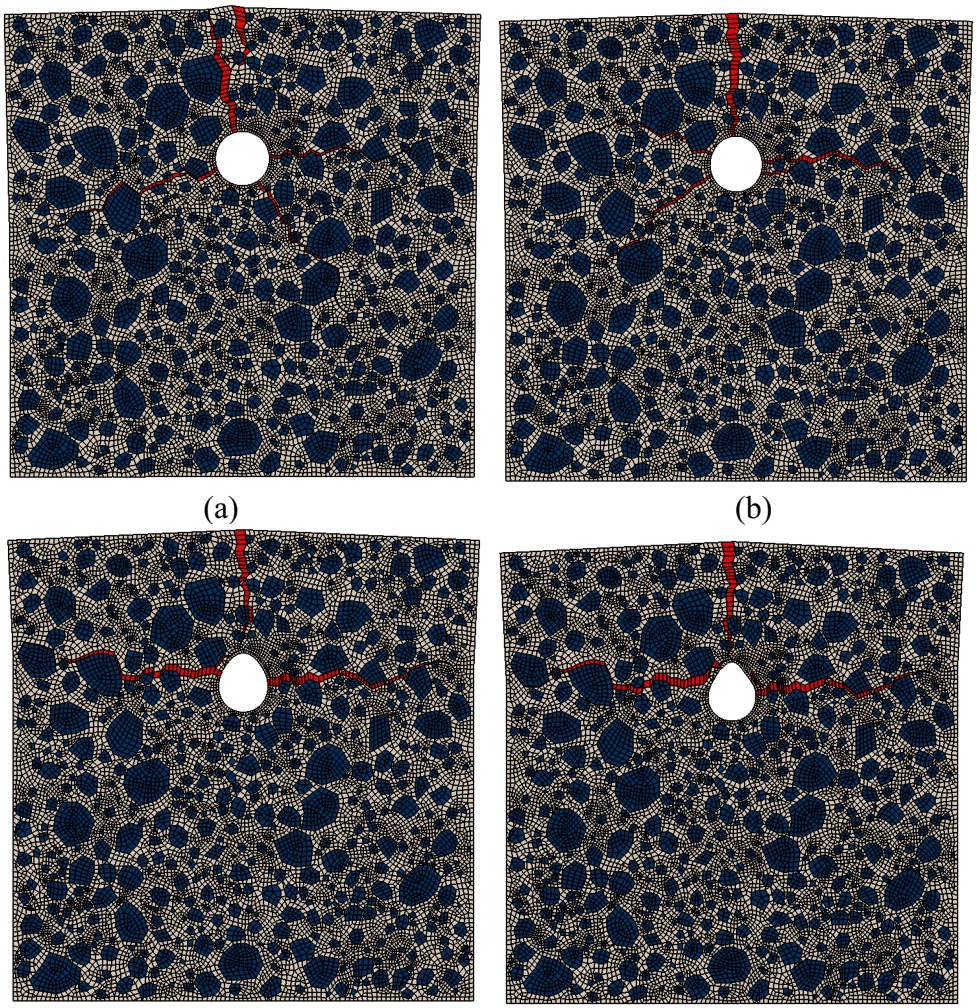

Figure 5 Concrete crack patterns induced by reinforcement corrosion for: (a) k=0; (b) k=1.28; (c) k=3.28; (d) k=5.94. The deformation scale is 10. Elements in red are cracked cohesive elements with damage values larger than 0.99.

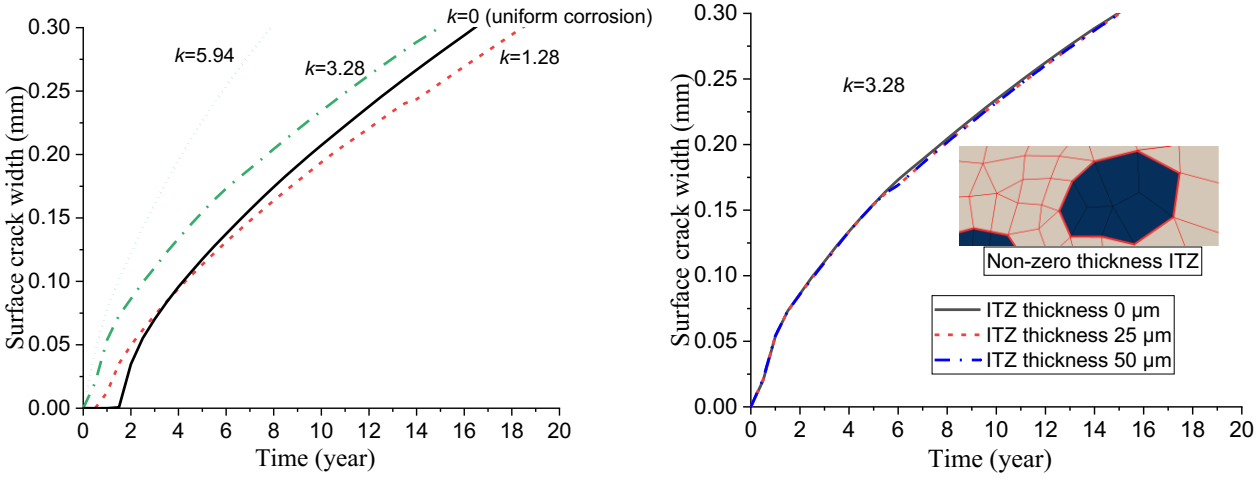

Figure 6 Crack width developments as a function of time affected by (a) non-uniform coefficient; (b) ITZ thickness

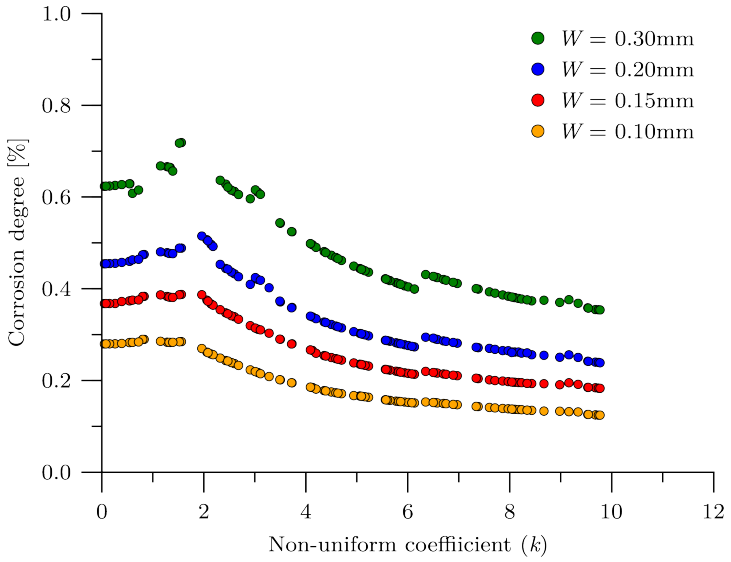

Figure 7 Corrosion degrees to crack widths reaching critical values affected by the non-uniform corrosion coefficient

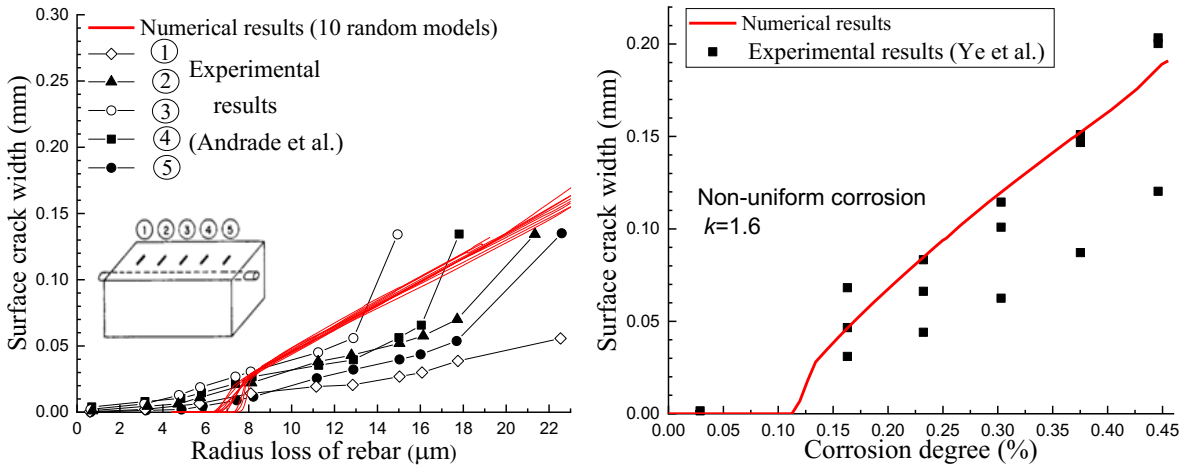

(a) (b)

Figure 8 Comparison of the crack width from numerical and experimental results: (a) uniform corrosion [56]; (b) non-uniform corrosion [57]

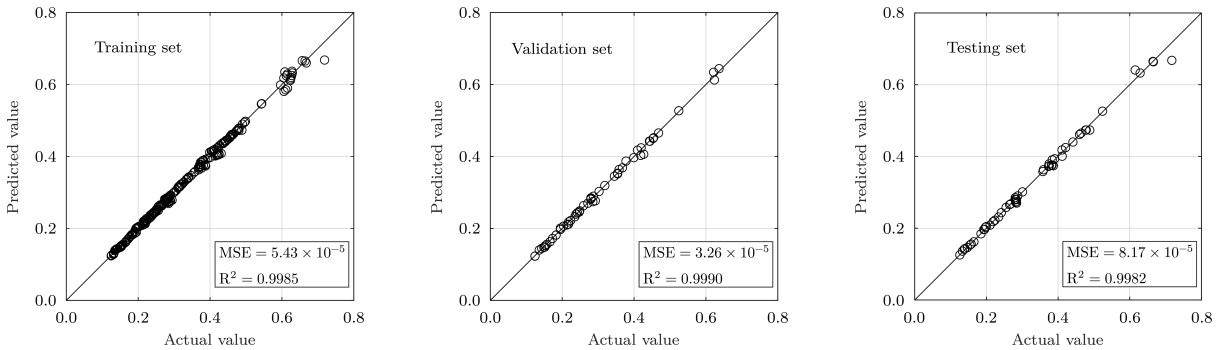

Figure 9 Correlation plots between numerical simulation (actual value) and surrogate model (predicted value)

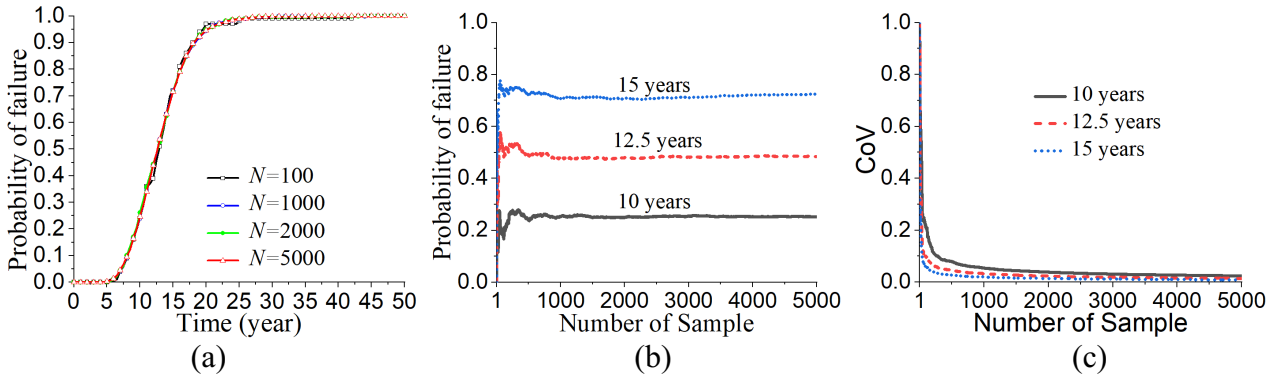

Figure 10 Time-dependent probability of failure predicted based on different sampling numbers: (a) time-dependent failure probability; (b) failure probability at different years; (c) COV of failure probability

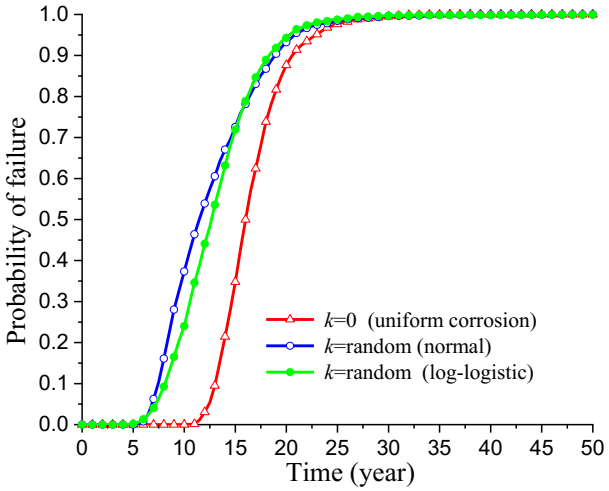

Figure 11 Effect of corrosion model on cracking failure

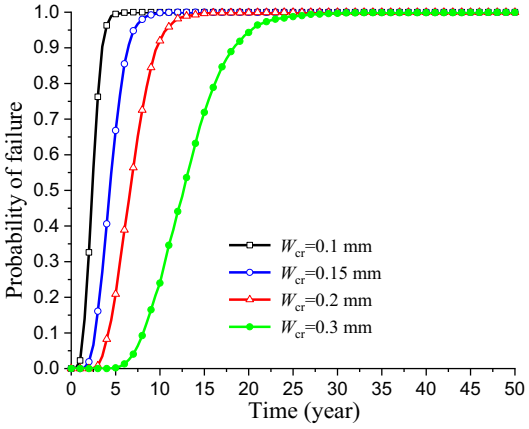

Figure 12 Effect of critical crack width on cracking failure

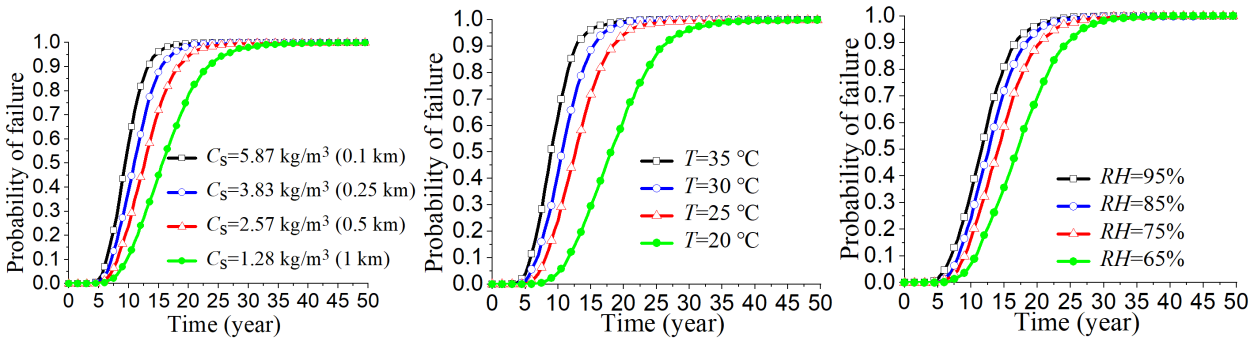

(a) (b) (c)

Figure 13 Effect of environmental parameters on cracking failure: (a) surface chloride content; (b) temperature; (c) relative humidity

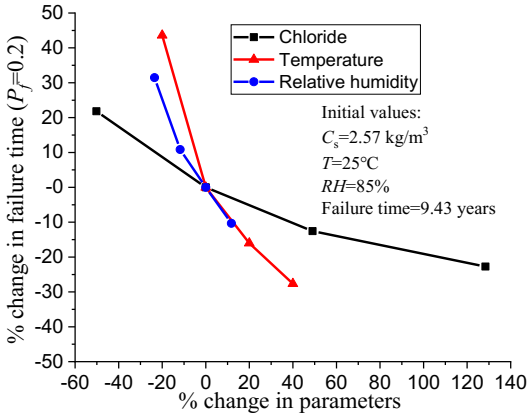

Figure 14 Sensitivity of failure to the environmental parameters